Automatic morphological detection of otolith nucleus

Frédéric Cao, Patrick Bouthemy, Ronan Fablet

Automatic morphological detection of otolith nucleus

Frédéric Cao, Patrick Bouthemy, Ronan Fablet

Abstract

*This paper deals with the analysis of otolith images for fish ageing issues. We present a new and well-founded approach for the automatic detection of the nucleus within otolith images. This topic is of key interest since the knowledge of the location of the otolith nucleus is required to achieve further processing (2*D *ring segmentation, age and growth estimation,...). Using morphological features within an* a contrario *framework, we develop a robust parameterless scheme. Its efficiency is demonstrated by an evaluation carried out for a set of several hundred of plaice otoliths.*

1 Problem statement

The acquisition of age and growth data is of key interest for marine living stock assessment and ecology applications. It relies on the interpretation of calcified structures, mainly otoliths (inner ears of the fish), routinely and manually performed by experts for several thousand of samples a year. Digital imaging offers new possibilities to ease the processing of these tedious tasks in a fully or partially automatic way [8, 11]. As illustrated by Fig.1 for a plaice otolith, otolith interpretation for ageing purposes comes to the analysis of yearly alternated opaque and translucent concentric rings. Determining the position of the otolith growth center is obviously a crucial issue, since it serves as the reference point. However, methods targeted at image-based automatic ageing [3, 4, 9, 12, 14] generally ignore this step to focus on the detection of the rings given the location of the otolith nucleus (also referred as the otolith center in the subsequent).

This paper presents a new and well-founded framework to reliably determine the position of the otolith center, such that it can be used for further analysis. This topic has only been considered in [4, 14]. The solution proposed in [14] simply resorts to the detection of the darkest point within a predefined area of interest set *a priori*. Experiments will show its rather low robustness. In [4], the detection of the otolith center is a by-product of the extraction of 2D growth rings. Though interesting, its main drawback lies in the overcomplex parametrization of the underlying multi-agent system. Contrarily, our scheme combines morphological features to the *a contrario* setting to perform a parameterless detection of otolith nucleus. The subsequent is organized as follows. Section 2 details the proposed morphological approach. Experiments, in particular a quantitative evaluation including a comparison to previously proposed approaches [4, 14] for a large set of Plaice otoliths, are presented in Section 3.

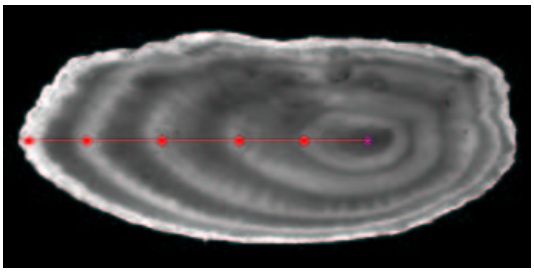

Figure 1. *Illustration of Plaice otolith interpretation for a 4 year old individual. a) Image of the Plaice otolith acquired under a binocular with transmitted light. The interpretation of the winter translucent rings is displayed by the markers set on the radial drawn on the main reading axis. b) Associated growth pattern (distance from the otolith center to the last ring as a function of the age).*

2 Proposed method

2.1 Topographic map

Let u be a grey level image. Its upper (resp. lower) level set at value λ is $\chi_\lambda(u) = \{x \in \mathbb{R}^2, u(x) \geq \lambda\}$ (resp. $\chi^\lambda(u) = \{x \in \mathbb{R}^2, u(x) \leq \lambda\}$). It is a classical result of Mathematical Morphology [5, 10] that these level sets give a complete representation of , which, in addition, is invariant with respect to global contrast changes. Level lines are the topological boundaries of connected components of level sets, and the topographic map is the collection of all level lines. The topographic map also characterizes the image, up to an increasing contrast change. Since level sets are nested, they can be embedded in a tree structure, computed by an

efficient algorithm due to Monasse and Guichard [7]. They call shape the interior of any level line. There are superior (resp. inferior) shapes, following whether they are obtained from an upper (resp. lower) level set. The denomination of shapes is due to the fact that they often correspond to shapes or part of shapes in real images [1].

2.2 Nucleus detection

Let us first remark that the otolith itself can be easily extracted as the largest shape in the image, that we shall denote by S_0. This is not very strict an hypothesis, since the acquisition of otolith images is well controlled, and the otolith is usually observed as it lies on a nearly constant background. To detect the nucleus, let us state the following qualitative facts: otoliths are vaguely elliptic, and nucleui correspond to a dark region close to the longest principal axis of the otolith. This region is also basically elliptic and no too excentric.

2.2.1 Maxima removal

Let us first express the fact that the nucleus corresponds to a dark region. Let $\mathcal{S}_0$ be the shapes included in S_0 (that is, part of the otolith). We also denote by $\mathcal{S}_1$ the set of shapes in $\mathcal{S}_0$ that does not contain any superior shape. In other terms, shapes in $\mathcal{S}_1$ do not contain any local maxima. Of course, this is a bit strict, since noise creates lots of them. Thus, we first apply a grain filter [13, 6], to the image, which consists in removing shapes whose area is less than a given threshold. This scale parameter is the unique parameter of our method. Its value is not sensitive since the size of the nucleus is always of few hundreds pixels. The size of the grain filter was set to the same value for all our experiments. Grain filter and maxima elimination leave of few dozens candidate shapes.

2.2.2 Principal axis proximity

Let us now denote by Δ the first principal axis of the otolith. Let D be a perpendicular axis to Δ, and $(X_i)_{i\in I}$ be a finite family of connected compact sets. Let X be one of the X_i. We say that X has a minimal distance to Δ on D if and only if $D \cap X \neq \emptyset$ and

$$d(D \cap \Delta, D \cap X) = \min_{i\in I} d(D \cap \Delta, D \cap X_i). \quad (1)$$

In (1), we measure the distance between a point $(D \cap \Delta)$ and and set $(D \cap X_i)$. This condition simply means that if we restrict the observation on D, then X is the closest to Δ. Finally, we say that $S \in \mathcal{S}$ if $S \in \mathcal{S}_1$ and if for any axis D, perpendicular to Δ such that $S \cap D \neq \emptyset$, then there exists $S' \in \mathcal{S}_1$ such that S' has a minimal distance to Δ on D among the shapes of $\mathcal{S}_1$ and $S \subset S'$.

The interpretation is much simpler that this formal geometrical definition: basically, if we start from Δ and move along its normal, then the first dark shape that we encounter must contain S.
While the first step remove bright shape, this second one removes elongated shapes that turn around the nucleus, while staying afar. (See Fig. 2.)

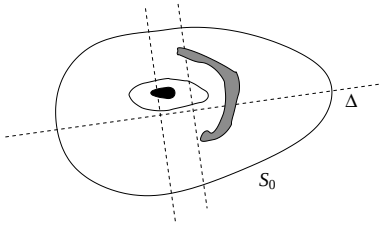

Figure 2. *Proximity to principal axis. The black-filled shape is in $\mathcal{S}$ since in any direction orthogonal to Δ, the only shape closest to Δ contains it. For the same reason, the white shape belongs to $\mathcal{S}$. On the contrary, one can find a normal to Δ such that the grey-filled shape is not the closest to Δ. Thus it does not belong to $\mathcal{S}$.*

2.2.3 Geometrical statistical selection

Among the remaining few candidates, we would like to choose the largest, the closer to Δ and the most circular shape. Fixing thresholds for geometrical quantities may be a bit dangerous since, even though otolith images are perceptually very alike, they enjoy a great variability of details. The two preceding steps are only qualitative, and avoid any threshold. They are also quite general and experimentally very stable. We now aim at

1. finding the best nucleus candidate.
2. giving a reliability measure to this detection.

Let us define three functions $(f_i)_{i=1,2,3}$ representing the three geometrical qualities of a good nucleus. The first one is the area

$$f_1(S) = |S|. \quad (2)$$

The second one is

$$f_2(S) = \frac{|S|}{\max_{x\in S} d(x,\Delta)^2}. \quad (3)$$

This function is scale invariant and measure how S is close to Δ, relatively to its size.
Let us now denote by $D(S, \Delta^\perp)$ the diameter of the projection of S on the orthogonal direction to Δ. We define

$$f_3(S) = \frac{|S|}{D(S,\Delta^\perp)^2}. \quad (4)$$

This value is also dimensionless, and describes the "flatness" of S with respect to the direction Δ. Let us remark that a good nucleus candidate will simultaneously yield large values of the f_i, in the case our geometrical qualitative assumptions hold. Let us make the *a contrario* hypothesis that the f_i are statistically independent. This assumption is reasonable for any shape except for the nucleus. A natural way to detect this independence violation is as follows: let us fix some values λ_i and calculate, under the independence assumption, the expected number of shapes assuming values of the f_i larger than λ_i. Whenever this value is lower than 1 and a shape S satisfies $f_i(S) \geq \lambda_i$, then chance alone cannot explain the observation. This is related to the Helmholtz principle, introduced by Desolneux, Moisan and Morel [2]. For $i = 1, 2, 3$, let

$$H_i(\mu) = \frac{\#\{S \in \mathcal{S},\ f_i(S) > \mu\}}{\#\{S \in \mathcal{S}\}}. \tag{5}$$

Definition 1 *Let $S \in \mathcal{S}$ and*

$$E(S) = \prod_{i=1}^{3} H_i(f_i(S)). \tag{6}$$

We define the nucleus N as the shape in $\mathcal{S}$ such that

$$E(N) = \min_{S \in \mathcal{S}} E(S). \tag{7}$$

This definition means that the best candidate is the less probable under the independence assumption. Of course, it may happen that only one of the probabilities H_i is small. Nevertheless, since the number of shape that are used in the histogram learning is small, we cannot estimate very small marginal probabilities. Thus, the most efficient way to have a small value of E is to have small values of H_i for all i. In practice, we learn the histogram on a set of about 100 shapes, yielding positive marginals greater than 10^{-2}. In practice, the minimizer of E in our experiments assumes a value between 10^{-4} and 10^{-5}. Remark that, following Desolneux et al., E provides a rejection threshold.

Definition 2 *We call number of false alarms (NFA) of S the number*

$$NFA(S) = \#\mathcal{S} \cdot E(S). \tag{8}$$

We also say that S is ε-meaningful if $NFA(S) < \varepsilon$.

The additivity of expectation immediately gives the following result (see [2]).

Proposition 1 *The expectation of the number of ε-meaningful shapes in the independence model is smaller than ε.*

As a consequence, if we choose $\varepsilon \geq 1$ and observe that a shape has a NFA larger than ε, we cannot conclude that it contradicts the independence assumption since the expected number of such an event may be comparable to ε.

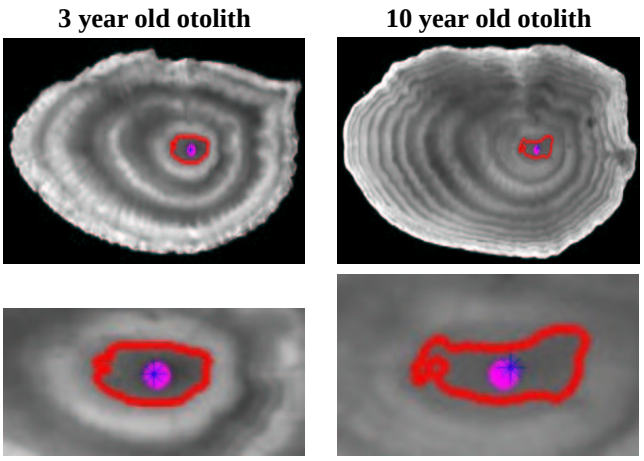

Figure 3. *Two examples of the detection of otolith center using our morphological approach: the red line depicts the contour of the selected shape, the blue star the estimated position of the otolith center, and the magenta circle its true position. The first row displays the image of the whole otolith, while the second row zooms in to the region close to the otolith center.*

3 Results

3.1 Examples

We first display two examples of the detection of the nucleus within otolith images for plaice samples. Fig.3 reports these two detections, the first one for a 3 years old otolith and the second one for a 10 years old one. The red line outlines the shape selected by our morphological approach, the blue star the estimated position of the nucleus and the magenta circle its actual position manually pointed out. The second row zooms in around the otolith center. In both cases, the selected shape is actually located within the first translucent ring. Consequently, an accurate estimation of the position of the otolith center is deduced. An important feature stresses by these two examples is the robustness of the morphological detection to the increase in image complexity in terms of the number of concentric seasonal rings.

3.2 Performance evaluation

We have carried out an evaluation of the proposed technique on a set of 250 images of Plaice otoliths belonging to age groups from 1 to 13. For each image, the position of the nucleus has been manually pointed out to provide the ground truth. To achieve a quantitative analysis of the detection performance, we define the rate of correct detection w.r.t. the threshold value λ as follows. Given an image, the detection of the otolith center is considered as correct

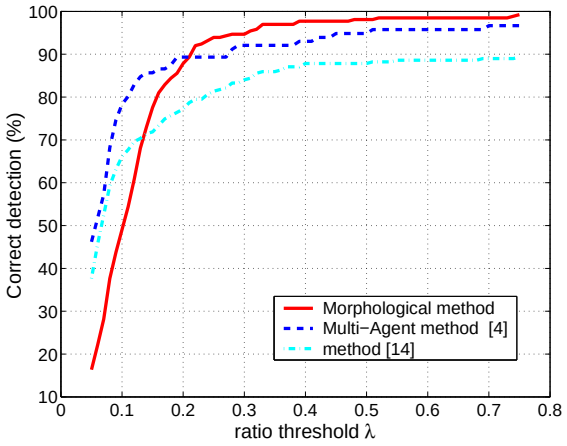

Figure 4. *Detection performance on a set of 250 Plaice otolith images. We evaluate the rate of correct detection for a range of values of the threshold λ (see text for details) for three techniques: the morphological approach presented in this paper (red line), the multi-agent technique introduced in [4] (blue – line) and the scheme used in [14] (cyan -. line). in terms of difference between the true and predicted positions of the otolith center. Markers + refer to the results supplied by the scheme used in [14], while the detections performed by our approach are displayed by markers o. The three methods need a CPU time about 1s per image.*

if the distance between the detected nucleus and the actual one is lower than λ times the distance from the actual nucleus center to the first translucent ring. For λ from 0 to 0.3, a correct detection can be regarded as very accurate. Besides, for $\lambda = 1$, it indicates whether or not the estimated position of the nucleus is within the first translucent ring. In addition, we compare the proposed morphological approach to the ones proposed in [4] and [14]. Fig.4 depicts the overall evaluation in terms of rate of correct detection with $\lambda \in [0, 0.8]$.

With correct detection rates close to 95% for $\lambda = 0.3$ and to 99% for $\lambda = 1$, the morphological approach performs robust and accurate detection of the otolith center. These promising results indicate that this scheme could be used as a preprocessing for further analysis, such as automatic ageing [3, 4], or for routine ageing issues.

Compared to previously proposed approaches, the morphological scheme largely outperforms the heuristic one used in [14], which simply consists in retrieving the darkest point within a predefined window, and also shows better performances than the multi-agent technique [4] (respectively, 94.8% 92.1% and 84% of correct detection for $\lambda = 0.3$). The close comparison of the morphological and multi-agent frameworks indicates that the latter is significantly less robust to detect the nucleus region, but may be more accurate when this detection points out to the relevant area of interest. Besides, whereas multi-agent systems are known to involve quite complex parametrization, the proposed morphological can be regarded as parameterless. It only requires to set the parameter value of the grain filter, used to filter out small regions. In our experiments, this value was set to 500 and the detection performances were shown to remain stable for a grain parameter within $[100, 600]$.

References

[1] V. Caselles, T. Coll, and J.M. Morel. Topographic maps and local contrast changes in natural images. *International Journal of Computer Vision*, 33(1):5–27, 1999.

[2] A. Desolneux, L. Moisan, and J.M. Morel. A grouping principle and four applications. *IEEE Transactions on Pattern Analysis and Machine Intelligence*, 25(4):508–513, 2003.

[3] R. Fablet, A. Benzinou, and C. Doncarli. Robust time-frequency model estimation in otolith images for fish age and growth analysis. In *Proc. of 10th Int. Conf. on Image Processing, ICIP'03*, Barcelona, Sept. 2003.

[4] A. Guillaud, A. Benzinou, H. Troadec, V. Rodin, and J. L. Bihan. Autonomous agents for edge detection and continuity perception on otolith images. *Image and Vision Computing*, 20(13-14):955–968, 2002.

[5] G. Matheron. *Random Sets and Integral Geometry*. John Wiley N.Y., 1975.

[6] P. Monasse. *Morphological Representation of Digital Images and Application to Registration*. PhD thesis, Université Paris IX Dauphine, 2000.

[7] P. Monasse and F. Guichard. Fast computation of a contrast invariant representation. *IEEE Transactions on Image Processing*, 9(5):860–872, 2000.

[8] A. Morison, S. Robertson, and D. Smith. An integrated system for production fish aging: image analysis and quality insurance. *North American Journal of Fisheries Management*, 18:587–598, 1998.

[9] S. Robertson and A. Morison. Development of an artificial neural network for automated age estimation. Technical Report 98/105, Marine and Freshwater Resources Institute, 1998.

[10] J. Serra. *Image Analysis and Mathematical Morphology*. Academic Press, 1982.

[11] G. Small and G. Hirschhorn. Computer-assisted age and growth pattern recognition of fish scales using a digitizing tablet. In G. H. R.C. Summerfelt, editor, *Age and Growth of Fish*, pages 397–410. ISU Press, 1987.

[12] H. Traodec, A. Benzinou, V. Rodin, and J. L. Bihan. Use of deformable templates for otolith 2D growth ring detection by digital image processing. *Journal of Fisheries Research*, 46(1-3):155–163, 2000.

[13] L. Vincent. Grayscale area openings and closings, their efficient implementation and applications. In J. Serra and P. Salembier, editors, *Proceedings of the 1^{st} Workshop on Mathematical Morphology and its Applications to Signal Processing*, pages 22–27, Barcelona, Spain, 1993.

[14] H. Welleman and F. Storbeck. Automatic ageing of Plaice otoliths by means of image analysis. In D. Secor, J. Dean, and S. Campana, editors, *Recent developments in Fish Otolith Research*, pages 271–282. Univ. of South Carolina Press, 1995.